Parallel RF Pulse Design with Subject-Specific Global SAR Supervision

C. M. Deniz[1,2], L. Alon[1,2], R. Brown[1], H-P. Fautz[3], D. K. Sodickson[1], and Y. Zhu[1]
[1]Center for Biomedical Imaging, Department of Radiology, NYU School of Medicine, New York, NY, United States, [2]Sackler Institute of Graduate Biomedical Sciences, NYU School of Medicine, New York, NY, United States, [3]Siemens Medical Solutions, Erlangen, Germany

Introduction: Electric field (**E** field) interferences inside the body have a strong influence upon the specific absorption rate (SAR) of parallel transmission RF pulses, and these interferences must be taken into account in order to manage SAR with confidence [1]. Using simulations of particular experimental conditions, SAR benefits of including measured **E** field interactions in RF pulse design for parallel transmission was shown in Ref. [2]. Subject-specific **E** field interactions can be measured via forward and reverse power readings as described in Ref. [3,4]. In this work, calibrated **E** field interactions in a phantom were incorporated into the design of parallel RF transmission pulses with minimal global SAR. The benefits of incorporating global SAR calibration information into RF pulse design were then validated using phantom experiments.

Methods: Experiments were performed on a Siemens whole body 7T Magnetom scanner (Erlangen, Germany) equipped with an eight-channel parallel transmit system. An eight-channel custom-built stripline coil array with elements disposed around the circumference of a 27.9cm-diameter cylinder was used for RF excitation and reception. Measurements were performed on 7.3-L cylindrical water phantom with 15cm diameter containing 1.25mg/L $NiSO_4.6H_2O$ and 4mg/L NaCl. Forward and reflected power readings in eight channels with sampling rate of 10μs were obtained with a power sensor (Rhodes&Schwarz, NRP-Z11) connected to directional couplers at the output of each RF amplifier via an RF switch (National Instruments, Dual 16x1 MUX). B_{1+} calibration was performed following the method described in Ref. [5]. ΔB_0 was measured using the phase information of two gradient-echo images with different TE values (TE_1, TE_2 = 7.14, 5.1ms) and incorporated into RF pulse design (Fig. 1b).

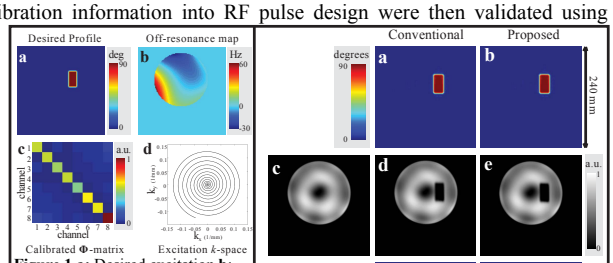

Figure 1 a: Desired excitation **b**: Measured off-resonance map. **c**: Calibrated power correlation matrix **d**: Variable density spiral k-space

The linear class LTA method [6] was used to design 90° excitation parallel RF pulses by solving Eq. 1, where $\mathbf{b}_{full}$ is the RF pulse waveform of all coils, **W** is the weighting matrix (equal to unity inside the phantom and zero elsewhere), $R(\mathbf{b}_{full})$ is the regularization term, "*" denotes the complex conjugate and $\mathbf{S}_{full}$ is the system matrix defined on Ref. [6]. The target excitation flip angle distribution $\boldsymbol{\theta}_{des}$ (Fig. 1a) was a homogenous 4x2cm^2 rectangular 2D profile blurred by convolving with a Gaussian kernel of FWHM = 1.2 cm to reduce ringing artifacts in the resulting magnetization distribution. Conventional Tikhonov regularization, Eq. 2, where β is used to trade off the excitation error against the integrated squared amplitude of the RF pulse waveform, is widely used in RF pulse design. The alternative regularization term in Eq. 3 was used for our global-SAR-optimized RF pulse design, which incorporates the constructive and destructive **E** field interferences that are ignored by conventional regularization terms. **Φ** is the power correlation matrix with elements shown in Eq. 4, L is the number of coil elements and the β parameter is now used to trade-off the excitation error against true global SAR. Experimental-setup-specific calibration of the **Φ** matrix (Fig. 1c) was performed using the automated power prediction and measurement technique described by Zhu [3] and by Alon et al. [4].

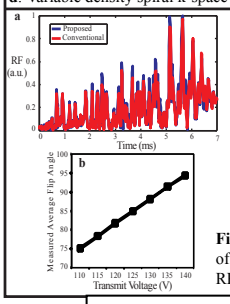

Figure 3 a: Amplitude of the designed RF pulses in one of the transmit channels. **b**: Linearity of the system and RF pulse design process with respect to transmit voltage

Figure 2 a, b: Bloch simulation results of the NRMSE aligned RF pulses calculated with conventional and proposed regularization terms. **d, e**: Scanner images obtained using RF pulses designed with the conventional and the proposed approach as a pre-saturation pulse over reference image (**c**). **f**: Flip angle map of the conventional RF pulse design with transmit voltage 135V. **g**: Flip angle map of the proposed global-SAR optimized

$$1)\ \hat{\mathbf{b}}_{full} = \arg\min_{\mathbf{b}^*_{full}} \{ \left\| \mathbf{S}_{full}\mathbf{b}^*_{full} - \boldsymbol{\theta}_{des} \right\|^2_{\mathbf{W}} + R(\mathbf{b}^*_{full}) \}$$

$$2)\ R(\mathbf{b}_{full}) = \beta \mathbf{b}^H_{full}\mathbf{b}_{full} \qquad 4)\ \Phi_{i,j} = \frac{1}{2}\int_V \sigma \mathbf{E}^*_i \cdot \mathbf{E}_j dv$$

$$3)\ R(\mathbf{b}_{full}) = \beta \mathbf{b}^H_{full}\boldsymbol{\Phi}^*_{full}\mathbf{b}_{full} \text{ where } \boldsymbol{\Phi}_{full} = \begin{bmatrix} \boldsymbol{\Phi} & & 0 \\ & \ddots & \\ 0 & & \boldsymbol{\Phi} \end{bmatrix}_{N_L x N_L}$$

A variable density inward spiral trajectory (Fig. 1d) with acceleration factor of 3 was used to cover excitation k-space. Two different regularization terms, containing the conventional identity matrix, **I**, or our proposed calibrated **E** field correlation matrix, $\boldsymbol{\Phi}_{full}$, were used to design parallel RF pulses. In simulations, normalized mean square error (NRMSE) between the magnetization distribution obtained from a Bloch simulator and the desired magnetization distribution was equalized using distinct heuristically chosen regularization parameters, β, so as to insure fair comparisons of SAR performance for equivalent excitation fidelity. In phantom experiments, flip angle profiles of the designed RF pulses were measured using the same B_{1+} calibration technique [5] used to construct $\mathbf{S}_{full}$. NRMSE and flip angle alignment between both design schemes was achieved inside the region where the desired rectangular magnetization profile (Fig. 1a) has flip angle values greater than 0°. Both regularization approaches were compared using the actual forward and reflected power readings of the system, while playing calculated parallel transmission RF pulses.

Table: Comparison of conventional and proposed parallel RF pulse design methods in terms of mean flip angle, NRMSE, and measured power.

	Proposed Parallel RF Pulse Design				Conventional Parallel RF Pulse Design			
Transmit Voltage (V)	**120**	**125**	**130**	**135**	**130**	**135**	**140**	**145**
Mean Flip Angle	81.7	84.9	88.1	91.4	85.5	88.7	91.8	94.8
NRMSE	1.58	1.61	1.64	1.67	1.62	1.65	1.68	1.71
Measured Power (W)	168	182	197	213	197	212	228	246

Results: Figures 2a and 2b represent the Bloch-simulated results of flip angle profiles calculated with conventional and proposed regularization terms, respectively. Both approaches resulted in NRMSE of 0.0319. The amplitude of the designed RF pulses of one of the channels is shown in Fig. 3a, which demonstrates that incorporating the **Φ**-matrix into RF pulse design results in local changes in the RF pulse waveform to improve the SAR management of the pulse as a whole while preserving excitation fidelity.

Calculated RF pulses were used as a pre-saturation pulse over a reference image obtained with RF shimming (Fig. 2c). Stepping through a range of transmit voltages (110V-150V), mean flip angle and NRMSE alignment between both design schemes was achieved. The table shows the measured mean flip angle and NRMSE values of both RF design schemes for different transmit voltages. For the given input transmit voltage range, the LCLTA parallel transmit RF pulse design resulted in a linear response of the system (Fig. 3b). This validates the linear class assumption used in the pulse calculation and the linearity of the system with the given input voltage range. Pre-saturation effects resulting from the designed 90° RF pulses can be seen in Figures 2d and 2e for 135V and 130V transmit voltages of RF designs with conventional and proposed regularization terms, respectively. Rectangular black regions within the phantom correspond to the desired magnetization region with 90° flip angle. Figure 2f and 2g show the magnitude flip angle maps of the designed RF pulses which were extracted from the ratio between reference and pre-saturation images. It is clear from the figure that there is a good agreement between Bloch simulations and experimental results. For the measured flip angle maps, calculated mean flip angle/NRMSE ratios were 88.14/1.65 and 88.67/1.64 for RF pulses designed with conventional (transmit voltage 135V) and proposed (transmit voltage 130V) regularization terms, respectively. The forward and the reflected power of the designed RF pulses were measured using the powermeter. The average net power measurements from the RF power amplifiers are shown in the Table for various transmit voltages. Measured average net power for RF designs was 212W with conventional and 197W with proposed regularization terms. Including global SAR calibration information into RF pulse design via regularization resulted in ~7% decrease in average net power deposition into the phantom.

Discussion: In this work, we have successfully demonstrated experimental reductions in RF power deposition resulting from inclusion of calibrated **E** field interferences within a regularization parameter in parallel excitation RF pulse. One significant limitation of our current setup is the location of the power sensor. At the back of the power amplifiers, the sensor gives power readings that have significant cable loss included - a separate measurement indicated that RF loss in the long connecting cables in our system accounts for over 50% of total RF power delivered by the RF power amplifiers. This significantly impacts the structure of the calibrated **Φ**-matrix, making the entries on the diagonal dominate. This setup can be improved and more significant SAR reduction can be realized [2] by moving the power sensing location close to the coil.

References: [1] Zhu, Y. (2004) MRM 51: 775-84. [2] Deniz CM (2010) ISMRM: 4930. [3] Zhu Y. (2009) ISMRM: 2585. [4] Alon L, et al. (2010): ISMRM 780. [5] Fautz, H-P et al. (2008) ISMRM: 1247. [6] Xu, D, et al.(2007) MRM 58: 326-34.